Statistical properties of the Mueller matrix of distributed targets

F.T. Ulaby
K. Sarabandi
A. Nashashibi

Indexing terms: Polarimetric radar, Remote sensing

Abstract: As a consequence of the reciprocity relation, the scattering matrix measured in the backscattering direction by a polarimetric radar system consists of five quantities: $|S_{vv}|$, $|S_{hh}|$, and $|S_{hv}|$, which are the magnitudes of the linearly polarised scattering amplitudes, and ϕ_c and ϕ_x, which are the co-polarised and crosspolarised phase angles. For statistically homogeneous, distributed terrain targets, the magnitudes are Rayleigh distributed and their means are related to the target's geometrical and dielectrical properties, but their normalised probability density functions are target independent. For most natural targets, the crosspolarised phase angle ϕ_x is uniformly distributed over $[0, 2\pi]$, and therefore contains no target-specific information. The co-polarised phase angle ϕ_c, on the other hand, is shown to exhibit a probability density function (PDF) that is characterised completely by two parameters α and ζ, both of which are related to the elements of the Mueller matrix of the target. The parameter α governs the width of the PDF and ζ governs the mean value of ϕ_c. It is further shown that the three magnitudes $|S_{vv}|$, $|S_{hh}|$, and $|S_{hv}|$ and the two parameters α and ζ completely specify the Mueller matrix, and therefore contain all the statistical information available from the polarimetric backscatter response of the target. These results are verified with experimental observations that show that α and ζ are related to the physical and dielectric properties of soil and vegetation targets.

1 Introduction

Unlike conventional SAR, which generates a high-resolution display of the radar backscattering coefficient of the imaged scene for the specific transmit-receive polarisation configuration used by the radar antenna, a coherent, polarimetric SAR measures the scattering matrix $\boldsymbol{S}$ (on a pixel by pixel basis) from which the scattering cross section σ (or scattering coefficient $\sigma^\circ = \sigma/A$, where A is the pixel area) can be computed for any desired transmit and receive polarisation combination through the application of the polarisation synthesis technique [1, 2]. Several models have recently been developed to characterise the polarimetric response of terrain, such as soil and vegetation-covered surfaces [3–5], with the expectation of using the models to extract more detailed information about the terrain from its polarimetric response than is available from conventional SAR data [6]. Because radar is a narrow-bandwidth coherent sensor, the radar image of a statistically homogeneous scene will exhibit 'speckle' due to signal fading scintillations [7], which usually necessitates spatial averaging of several pixels prior to interpreting the data. To apply the polarisation synthesis technique, one could follow either of two basic procedures. In the first procedure, the scattering cross section σ is synthesised for each pixel using the scattering matrix measured for that pixel, and then σ is averaged over however many pixels are deemed necessary for interpreting the data. In the second procedure, each of the measured (2 × 2) complex scattering matrices are first converted to their corresponding 4 × 4 real Mueller matrices (or Stokes scattering operators or Stokes covariance matrices), the averaging is performed over the 4 × 4 real matrices, and then the polarisation synthesis technique is applied to the averaged 4 × 4 matrix [1]. For a distributed target represented by many pixels in a radar image (such as an ocean surface, or a forest canopy), a coherent polarimetric radar offers two basic types of information: (*a*) the synthesised polarisation response, which represents the average scattering coefficient as a function of all possible combinations of transmit and receive antenna polarisations, and (*b*) the probability density functions of the magnitudes and polarisation phase differences (which are defined in the next Section). For statistically distributed targets, the magnitude of the backscattered signal is Rayleigh distributed regardless of the geometrical and dielectric properties of the target. Hence, only the mean value of the magnitude contains information about the target. The polarisation phase differences are ϕ_c and ϕ_x, where $\phi_c = \phi_{hh} - \phi_{vv}$ is the co-polarised phase angle, $\phi_x = \phi_{hv} - \phi_{vv} = \phi_{vh} - \phi_{vv}$ is the crosspolarised phase angle, and ϕ_{ij} is the phase of the received electric field for receive polarisation i and transmit polarisation j. The subscripts h and v refer to horizontal and vertical polarisation respectively. Experimental data acquired by coherent polarimetric SAR systems and by polarimetric scatterometer systems have shown that the crosspolarised phase angle ϕ_x is uniformly distributed over $[0, 2\pi]$ for any distributed target. Hence, ϕ_x does not contain information about the target. In contrast, the probability density function of ϕ_c is strongly dependent upon both

Paper 8616F (E15), first received 23rd April and in revised form 5th December 1991

The authors are with the Department of Electrical Engineering and Computer Science, College of Engineering, The University of Michigan, Ann Arbor, MI 48109-2122, USA

the sensor parameters (incidence angle and wavelength) and the target parameters (roughness, dielectric constant, geometry, etc.)

To measure the scattering matrix $\boldsymbol{S}$, the measuring radar system should maintain good phase stability over the duration of the measurement. Usually the four elements of $\boldsymbol{S}$ are measured by transmitting a linear polarisation, such as v, and recording both the h- and v-polarised backscattered signals, and then repeating the process after changing the transmit signal to h polarisation. This can be accomplished by alternating the polarisation of the transmitted pulses. The movement of a SAR between adjacent pulses results in some decorrelation between the received signals because they will not view exactly the same area on the ground. This problem can be corrected, however, by proper sampling and interpolation, albeit at the cost of increased complexity of the SAR signal processor.

The data available from a calibrated polarimetric SAR image of a statistically homogeneous distributed target can be used in either one of two forms. The first consists of the means of the three principal polarisation magnitudes, $\langle S_{vv} S_{vv}^* \rangle$, $\langle S_{hh} S_{hh}^* \rangle$ and $\langle S_{hv} S_{hv}^* \rangle$, and the PDF of ϕ_c, $f(\phi_c)$. The goal is to relate these quantities to the physical and dielectric properties of the target, with the ultimate objective being to invert the process so as to infer the properties of the target from the radar observations. The second form is the Mueller matrix $\boldsymbol{M}$, whose elements are given by ensemble averages of various products of the elements of the scattering matrix $\boldsymbol{S}$. The Mueller-matrix form is used for polarisation synthesis (which can also be realised from the measured $\boldsymbol{S}$ matrices directly), but more importantly it is the only means available for comparing measured data with theoretical models. Scattering models of the polarimetric response of terrain are inherently ensemble-average processes and their output products are expressions of the Mueller matrix, $\boldsymbol{M}$. Three of the elements of $\boldsymbol{M}$ are identical to the magnitudes mentioned earlier, but until recently, it was not possible to obtain $f(\phi_c)$ from $\boldsymbol{M}$. Hence, it was not possible to compare the measured $f(\phi_c)$ with theoretical predictions nor to evaluate the potential information about the target contained in $f(\phi_c)$. Based on a recent study by Sarabandi [8], $f(\phi_c)$ can be completely specified in terms of two parameters, α and ζ, both of which are given explicitly in terms of the elements of $\boldsymbol{M}$, thereby providing the missing link between the statistics of the polarimetric response available from the SAR measurements and the expressions for the Mueller matrix available from theoretical models. This is examined in the present paper and verified with experimental data for soil surfaces and small trees.

Another important application of the link between $f(\phi_c)$ and $\boldsymbol{M}$ pertains to nonfully coherent polarimetric radar techniques that measure $\boldsymbol{M}$ directly. At centimetre wavelengths SAR technology is capable of maintaining phase coherence at the level necessary for measuring the scattering matrix $\boldsymbol{S}$ with good magnitude and phase accuracy, but phase stability requirements are more difficult to achieve at the shorter millimetre wavelengths, particularly at the 140 and 215 GHz atomospheric window frequencies. These limitations have led researchers to develop an alternative measurement technique which requires the system to be able to measure the phase difference between the two simultaneously received orthogonal polarisation channels, but does not require phase stability from one pulse to the next [9–11]. This coherent-on-receive polarimetric radar technique does not measure the scattering matrix $\boldsymbol{S}$, but measures the Mueller matrix directly, instead.

2 Polarimetric response

The object located at the centre of the co-ordinate system shown in Fig. 1 is illuminated by a plane wave radiated by a transmitting antenna in the direction $\hat{\boldsymbol{k}}_t$. The angles (θ_i, ϕ_i) specify the direction of the unit vector $\hat{\boldsymbol{k}}_t$. In

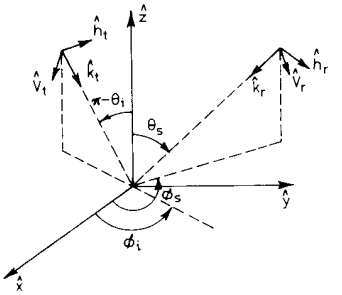

Fig. 1 *Co-ordinate systems and scattering geometry for the backscatter alignment (BSA) convention*

general the incident wave may be composed of a vertical polarisation component $\hat{\boldsymbol{v}}_t$ and a horizontal component $\hat{\boldsymbol{h}}_t$, defined such that the co-ordinate system $(\hat{\boldsymbol{k}}_t, \hat{\boldsymbol{v}}_t, \hat{\boldsymbol{h}}_t)$ coincides with the $(\hat{\boldsymbol{r}}, \hat{\boldsymbol{\theta}}, \hat{\boldsymbol{\phi}})$ of a standard spherical co-ordinate system. Although our interest is in the backscatter situation, wherein the transmit and receive antennas are co-located, the configuration shown in Fig. 1 corresponds to the general bistatic case, chosen for ease of illustration. The receive antenna observes the target in the direction $\hat{\boldsymbol{k}}_r$ and its polarisation unit vectors $\hat{\boldsymbol{v}}_r$ and $\hat{\boldsymbol{h}}_r$ are defined as if it were a transmitting antenna, in accordance with the backscatter alignment convention. Using this convention, in the backscatter case the angles shown are related by $\theta_s = \pi - \theta_i$ and $\phi_s = \pi + \phi_i$, and the transmit and receive unit vectors become coincident: $(\hat{\boldsymbol{k}}_t, \hat{\boldsymbol{v}}_t, \hat{\boldsymbol{h}}_t) = (\hat{\boldsymbol{k}}_r, \hat{\boldsymbol{v}}_r, \hat{\boldsymbol{h}}_r)$.

2.1 Scattering matrix

In general, the electric field of the plane wave radiated by the transmitting antenna is elliptically polarised with complex polarisation components E_v^t and E_h^t. Thus

$$\boldsymbol{E}^t = E_v^t \hat{\boldsymbol{v}}_t + E_h^t \hat{\boldsymbol{h}}_t \tag{1}$$

with the phase reference of $\boldsymbol{E}^t$ chosen to be at the centre of the illuminated target (i.e., at the centre of the co-ordinate system). The field of the spherical wave scattered by the target in the direction of the receive antenna, defined in terms of the polarisation vectors of the receive antenna, is given by

$$\boldsymbol{E}^r = E_v^r \hat{\boldsymbol{v}}_r + E_h^r \hat{\boldsymbol{h}}_r \tag{2}$$

and it is related to $\boldsymbol{E}^t$ by [12, 13]:

$$\boldsymbol{E}^r = \frac{e^{ikr}}{r} \boldsymbol{S}\boldsymbol{E}^t \tag{3}$$

where r is the distance between the target and the receive antenna and $\boldsymbol{S}$ is the scattering matrix of the scattering target,

$$\boldsymbol{S} = \begin{bmatrix} S_{vv} & S_{vh} \\ S_{hv} & S_{hh} \end{bmatrix} \tag{4}$$

The elements $\boldsymbol{S}_{ij}$ of $\boldsymbol{S}$ are called the scattering amplitudes, and the subscripts ij denote the polarisation configuration of the receive and transmit fields, in that order. To

measure the scattering amplitudes of a given target, one needs to use a coherent radar system with dual polarisation capability for both transmission and reception. Upon transmitting a vertically polarised wave $\boldsymbol{E}^t = E_v^t \hat{\boldsymbol{v}}_t$, and recording both components of the received wave (E_v^r and E_h^r) using a dual polarised antenna, the scattering amplitudes S_{vv} and S_{hv} can be determined from

$$S_{vv} = \left[\frac{e^{ikr}}{r}\right]^{-1} \frac{E_v^r}{E_v^t} \tag{5}$$

$$S_{hv} = \left[\frac{e^{ikr}}{r}\right]^{-1} \frac{E_h^r}{E_v^t} \tag{6}$$

The factor $[e^{ikr}/r]^{-1}$ can be determined by measuring the field backscattered from a target with known scattering matrix, such as a metallic sphere. A similar procedure involving the transmission of a horizontally polarised wave leads to the determination of S_{hh} and S_{vh}.

Each scattering amplitude S_{ij} is a complex quantity comprised of a magnitude $|S_{ij}|$ and a phase angle ϕ_{ij},

$$S_{ij} = |S_{ij}| e^{i\phi_{ij}}, \quad i, j = v \text{ or } h \tag{7}$$

and for backscattering, the reciprocity relation for polarised scattering mandates that the crosspolarised scattering amplitudes be equal,

$$S_{hv} = S_{vh} \tag{8}$$

Using eqns. 7 and 8, the scattering matrix can be written in the form

$$\boldsymbol{S} = e^{i\phi_{vv}} \begin{bmatrix} |S_{vv}| & |S_{vh}| e^{i\phi_x} \\ |S_{vh}| e^{i\phi_x} & |S_{hh}| e^{i\phi_c} \end{bmatrix} \tag{9}$$

where

$$\phi_x = \phi_{hv} - \phi_{vv} = \phi_{vh} - \phi_{vv} \tag{10}$$

$$\phi_c = \phi_{hh} - \phi_{vv} \tag{11}$$

thus referencing all phase angles to the phase angle of the vv-polarised element. We shall henceforth refer to ϕ_x and ϕ_c as the cross- and co-polarised phase angles, respectively.

2.2 Polarisation synthesis for a point target

With $\boldsymbol{S}$ known, the radar cross section (RCS) for any of the principal linear polarisation combinations can be obtained from

$$\sigma_{ij} = 4\pi |S_{ij}|^2; \quad i, j = v \text{ or } h \tag{12}$$

To compute the radar cross section for any other polarisation combination, we first need to define the polarisation vectors $\hat{\boldsymbol{p}}^t$ and $\hat{\boldsymbol{p}}^r$ of the transmit and receive antennas. If the field $\boldsymbol{E}$ that would be radiated by an antenna is

$$\begin{aligned} \boldsymbol{E} &= E_v \hat{\boldsymbol{v}} + E_h \hat{\boldsymbol{h}} \\ &= a_v e^{-i\delta_v} \hat{\boldsymbol{v}} + a_h e^{-i\delta_h} \hat{\boldsymbol{h}} \end{aligned} \tag{13}$$

where a_v and a_h are the magnitudes of the v- and h-polarised components and ϕ_v and ϕ_h are the corresponding phase angles, then the antenna polarisation vector, written in matrix form, is given by

$$\boldsymbol{p} = \frac{\boldsymbol{E}}{|\boldsymbol{E}|} = \begin{bmatrix} \cos\alpha \\ \sin\alpha e^{-i\delta} \end{bmatrix} \tag{14}$$

where $\tan\alpha = a_h/a_v$ and $\delta = \delta_h - \delta_v$. A factor of $e^{-i\delta_v}$ multiplying the matrix in eqn. 14 has been suppressed for convenience because it is not needed in the application of the polarisation synthesis technique. Often, wave polarisation is described in terms of the polarisation ellipse (Fig. 2), characterised by the rotation angle ψ and ellipticity angle χ, which are related to α and δ by

$$\tan 2\psi = (\tan 2\alpha) \cos\delta \tag{15}$$

$$\sin 2\chi = (\sin 2\alpha) \sin\delta \tag{16}$$

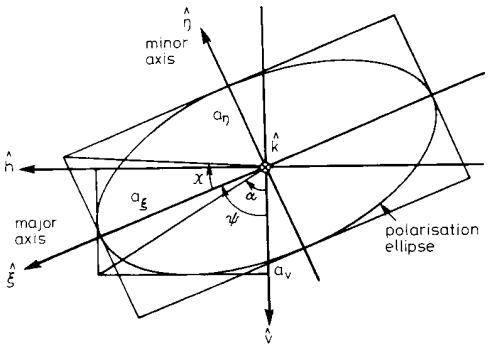

Fig. 2 *Polarisation ellipse in the v–h plane for a wave travelling in the $\hat{k}$ direction*

and conversely,

$$\cos 2\alpha = (\cos 2\chi)(\cos 2\psi) \tag{17}$$

$$\tan\delta = \frac{\tan 2\chi}{\sin 2\psi} \tag{18}$$

For a target with scattering matrix $\boldsymbol{S}$, its radar cross section can be computed for any receive and transmit polarisation, defined by the polarisation angles (ψ_r, χ_r) and (ψ_t, χ_t) — or equivalently, by the parameters (α_r, δ_r) and (α_t, δ_t) — by applying the polarisation synthesis equation [11]:

$$\sigma(\psi_r, \chi_r; \psi_t, \chi_t) = 4\pi |\boldsymbol{p}^r \cdot \boldsymbol{S}\boldsymbol{p}^t|^2 \tag{19}$$

2.3 Synthesis for a distributed target

Unlike point targets, soil surfaces and vegetation canopies are distributed targets, composed of randomly-distributed scatterers. The backscatter behaviour of a distributed target is characterised by the backscattering coefficient, σ^0, which is the ensemble average of the radar cross section, σ, per unit area,

$$\sigma^0 = \frac{\langle\sigma\rangle}{A} \tag{20}$$

where A is the illuminated area. For the principal linear polarisations, the synthesis process is straightforward: simply measure $\boldsymbol{S}$ for each of many independent samples of the distributed target (or pixels of resolution area A, in the case of an imaging radar), and then compute

$$\sigma_{ij}^0 = \frac{4\pi}{AN} \sum_{l=1}^{N} |S_{ij}|_l^2, \quad ij = v \text{ or } h \tag{21}$$

where N is the number of independent samples measured. For other polarisation combinations of transmit and receive polarisations, two approaches are available, both of which provide identical results.

Scattering matrix approach: The first approach is basically identical to the synthesis technique used in conjunction with point targets. Thus,

$$\sigma^{\circ}(\psi_r, \chi_r; \psi_t, \chi_t) = \frac{4\pi}{AN} \sum_{l=1}^{N} |\boldsymbol{p}^r \cdot \boldsymbol{S}_l \boldsymbol{p}^t|^2 \tag{22}$$

where $\boldsymbol{S}_l$ is the measured scattering matrix of the lth sample.

Stokes scattering operator approach: Instead of synthesising the backscatter N times and then averaging the sum to obtain σ^0, as outlined in the preceding approach, it is possible to use a computationally more efficient approach, based on the Stokes scattering operator [1, p. 32]. To show the procedure, we start with the modified Stokes vector representation of a polarised wave,

$$\boldsymbol{F}(\psi, \chi) = \begin{bmatrix} I_v \\ I_h \\ U \\ V \end{bmatrix} = \begin{bmatrix} \langle |E_v|^2 \rangle \\ \langle |E_h|^2 \rangle \\ \langle 2 \text{ Re } (E_v E_h^*) \rangle \\ \langle 2 \text{ Im } (E_v E_h^*) \rangle \end{bmatrix} \tag{23}$$

where $\langle\ \rangle$ denotes ensemble average. Upon applying eqn. 3, it can be shown [1] that the transmitted and scattered modified Stokes vectors are related by the modified Mueller matrix $\boldsymbol{M}$,

$$\boldsymbol{F}^r = \frac{1}{r^2} \boldsymbol{M} \boldsymbol{F}^t \tag{24}$$

with the elements of $\boldsymbol{M}$ being real quantities, given in terms of the elements of the scattering matrix $\boldsymbol{S}$,

$$\boldsymbol{M} = \left\langle \begin{bmatrix} |S_{vv}|^2 & |S_{vh}|^2 \\ |S_{hv}|^2 & |S_{hh}|^2 \\ 2 \text{ Re } (S_{vv} S_{hv}^*) & 2 \text{ Re } (S_{vh} S_{hh}^*) \\ 2 \text{ Im } (S_{vv} S_{hv}^*) & 2 \text{ Im } (S_{vh} S_{hh}^*) \end{bmatrix} \right.$$

$$\left. \cdots \begin{matrix} \text{Re } (S_{vh}^* S_{vv}) & -\text{Im } (S_{vh}^* S_{vv}) \\ \text{Re } (S_{hh}^* S_{hv}) & -\text{Im } (S_{hv} S_{hh}^*) \\ \text{Re } (S_{vv} S_{hh}^* + S_{vh} S_{hv}^*) & -\text{Im } (S_{vv} S_{hh}^* - S_{vh} S_{hv}^*) \\ \text{Im } (S_{vv} S_{hh}^* + S_{vh} S_{hv}^*) & \text{Re } (S_{vv} S_{hh}^* - S_{vh} S_{hv}^*) \end{matrix} \right\rangle \tag{25}$$

For a distributed target, the following polarisation synthesis equation is applicable [11]:

$$\sigma^{\circ}(\psi_r \chi_r; \psi_t, \chi_t) = \frac{4\pi}{A} \boldsymbol{A}^r \cdot \boldsymbol{Q} \boldsymbol{M} \boldsymbol{A}^t \tag{26}$$

where $\boldsymbol{A}^r$ and $\boldsymbol{A}^t$ are the normalised modified Stokes vectors for the receive and transmit antennas [$\boldsymbol{A} = \boldsymbol{F}/(I_v + I_h)$], A is the illuminated area, and $\boldsymbol{Q}$ is a diagonal transformation matrix given by

$$\boldsymbol{Q} = \begin{bmatrix} 1 & 0 & 0 & 0 \\ 0 & 1 & 0 & 0 \\ 0 & 0 & \frac{1}{2} & 0 \\ 0 & 0 & 0 & -\frac{1}{2} \end{bmatrix} \tag{27}$$

3 Statistical properties of the Mueller matrix

The polarisation synthesis capability provided by a polarimetric radar offers a number of obvious advantages, including the optimisation of the radar response to enhance discrimination between different types of terrain and the detection of point targets against the background clutter [1, Chapt. 7]. These applications, however, are not the subject of this paper.

The intent of this paper is to examine the statistical properties of the Mueller matrix $\boldsymbol{M}$. We start by defining each of the scattering amplitudes in terms of its real and imaginary components,

$$S_{vv} = |S_{vv}| e^{i\phi_{vv}} = \rho_1 e^{i\phi_{vv}} = x_1 + ix_2 \tag{28}$$

$$S_{hh} = |S_{hh}| e^{i\phi_{hh}} = \rho_2 e^{i\phi_{hh}} = x_3 + ix_4 \tag{29}$$

$$S_{hv} = |S_{hv}| e^{i\phi_{hv}} = \rho_3 e^{i\phi_{hv}} = x_5 + ix_6 \tag{30}$$

where $\rho_1 = |S_{vv}|$, $\rho_2 = |S_{hh}|$, $\rho_3 = |S_{hv}|$, and because of the reciprocity relation, $S_{hv} = S_{vh}$ for backscatter.

3.1 Statistics of the individual magnitudes and phases

When a radar illuminates a volume of a random medium or an area of a random surface, many point scatterers contribute to the total scattered electric field received by the radar. Hence, each of the scattering amplitudes is represented by a sum of the form

$$S_{pq} = |S_{pq}| e^{i\phi_{pq}} = \sum_{n=1}^{N} |S_{pq}^n| e^{i\phi_{pq}^n}, \quad p, q = v, h \tag{31}$$

where N is the total number of scatterers and $|S_{pq}^h|$ and ϕ_{pq}^n are the magnitude and phase angle of the field due to the nth scatterer. The phase angle ϕ_{pq}^n includes a phase delay related to the scatterer's location with respect to a reference position (such as the centre of the distributed target). Because the scatterers are randomly located within the illuminated volume (or area), the magnitude $|S_{pq}^n|$ and phase ϕ_{pq}^n are statistically independent variables. For N large, this independence leads to the result that the real and imaginary parts of S_{pq} are independent, zero-mean, Gaussian random variables with equal variances [7, p. 38–43]. For S_{vv}, for example, these properties can be shown to lead to the following probability density functions for the magnitude ρ_1 and phase angle ϕ_{vv} of S_{vv}

$$f_{\rho_1}(\rho_1) = \frac{\rho_1}{\lambda_{11}} \exp\left(-\frac{\rho_1}{2\lambda_{11}}\right) \tag{32}$$

$$f_{\phi_{vv}}(\phi_{vv}) = \frac{1}{2\pi} \tag{33}$$

where $\lambda_{11} = \langle x_1^2 \rangle = \langle x_2^2 \rangle = \lambda_{22}$ is the variance of both x_1 and x_2. The PDF given by eqn. 32 is the Rayleigh distribution with mean $\langle \rho_1 \rangle = \langle |S_{vv}| \rangle = \sqrt{(\pi \lambda_{11}/2)}$.

Experimental verification of the assumption that x_1 and x_2 are Gaussian-distributed random variables with equal variances is given in Fig. 3, which displays the PDFs of x_1, x_2, x_3, and x_4, based on approximately 1000 measurements of a random soil surface observed by a truck-mounted polarimetric scatterometer at 4.75 GHz. Similar results were also observed for the crosspolarised components x_5 and x_6.

The power, $\rho_1^2 = (S_{vv} S_{vv}^*)$, is characterised by an exponential distribution,

$$f_{\rho_1^2}(\rho_1^2) = \frac{1}{2\lambda_{11}} \exp\left(-\frac{\rho_1^2}{2\lambda_{11}}\right) \tag{34}$$

with mean value

$$\langle \rho_1^2 \rangle = \langle S_{vv} S_{vv}^* \rangle = 2\lambda_{11} = M_{11} \tag{35}$$

where M_{11} is the 11th element of the Mueller matrix given by eqn. 25. Because the PDF given by eqn. 34 is a

single-parameter distribution, the mean value M_{11} is sufficient for characterising the statistical behaviour of $|S_{vv}|^2$. Similar distributions and statements apply to the powers $|S_{hh}|^2$ and $|S_{hv}|^2$.

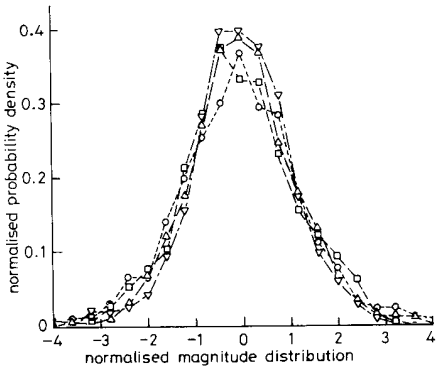

Fig. 3 *Histogram of the real and imaginary parts of S_{vv} and S_{hh} for a rough surface with rms height 0.32 cm and correlation length 9.9 cm at C-band and 30° incidence angle*

--○-- Real (S_{vv})
—□— Imag (S_{vv})
—△— Real (S_{hh})
—▽— Imag (S_{hh})

3.2 Statistics of the phase differences

Although individually the phase angles ϕ_{vv}, ϕ_{hh}, and ϕ_{hv} are uniformly distributed over $[-\pi, \pi]$, and therefore contain no information about the target's geometrical and dielectric properties, their differences $\phi_c = \phi_{hh} - \phi_{vv}$ and $\phi_x = \phi_{hv} - \phi_{vv}$ may not be uniformly distributed and may in fact be related to the target's properties. As will be discussed later, the crosspolarised phase angle ϕ_x is approximately uniformly distributed over $[-\pi, \pi]$ for most natural targets (such as soil surfaces and vegetation), but the copolarised phase angle ϕ_c is approximately Gaussian in shape with its mean and variance being directly related to the elements of the Mueller matrix $\boldsymbol{M}$.

Using the statistical properties of the scattering amplitudes given in the preceding section, closed form solutions are available in Appendix 8 for the probability density functions of ϕ_c and ϕ_x. The PDF of ϕ_c is given by (81)

$$f(\phi_c) = \frac{\lambda_{11}\lambda_{33} - \lambda_{13}^2 - \lambda_{14}^2}{2\pi(\lambda_{11}\lambda_{33} - D^2)} \left\{1 + \frac{D}{\sqrt{(\lambda_{11}\lambda_{33} - D^2)}} \times \left[\frac{\pi}{2} + \tan^{-1}\frac{D}{\sqrt{(\lambda_{11}\lambda_{33} - D^2)}}\right]\right\} \quad (36)$$

where

$$D = \lambda_{13}\cos\phi_c + \lambda_{14}\sin\phi_c \quad (37)$$

and the quantities λ_{13}, λ_{14}, λ_{11}, and λ_{33} are all expressed in terms of the elements of the Mueller matrix. The validity of eqn. 36 has been verified against experimental data for a variety of distributed targets using both truck-mounted radar measurements and airborne SAR observations. By way of illustration, we show in Fig. 4*a* a histogram of $f(\phi_c)$ based on direct measurements of ϕ_c for a slightly rough surface and a plot of $f(\phi_c)$ computed according to eqn. 36 and the measured Mueller matrix of the surface. Excellent agreement is observed between the measured histogram and the theoretical expression in terms of the shape of the PDF and the mean value and stadard deviation of ϕ_c. Similar remarks apply to Fig. 4*b* for the crosspolarised phase difference ϕ_x, for which the theoretical PDF was calculated using (84). The experimental data used in Fig. 4 were measured by a truck-mounted polarimetric scatterometer. An example depicting similar results based on airborne SAR observations of grass-covered terrain is shown in Fig. 5.

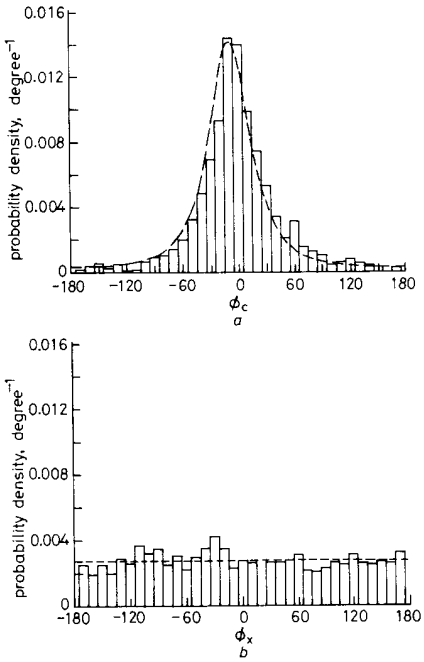

Fig. 4 *Measured and calculated probability density functions*

a the co-polarised phase angle $\phi_c = \phi_{hh} - \phi_{vv}$
——— Measured (Mean = −5.0°, Std. Dev. = 47.7°)
- - - - Calculated (Mean = −7.8°, Std. Dev. = 47.2°)
b the cross-polarised phase angle $\phi_x = \phi_{hv} - \phi_{vv}$. The target is a slightly rough soil surface with rms height of 0.32 cm, observed at a frequency of 4.75 GHz and incidence angle of 30°
——— Measured (Mean = −1.0°, Std. Dev. = 102.5°)
- - - - Calculated (Mean = 0.8°, Std. Dev. = 103.7°)

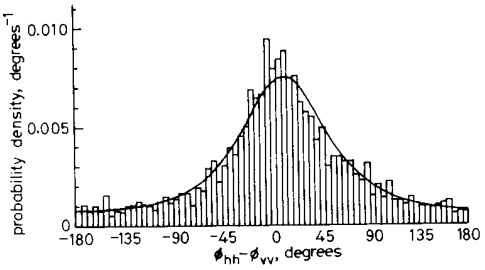

Fig. 5 *Measured and calculated $f(\phi_c)$ for a grassy area in Northern Michigan observed by a 1.2 GHz SAR in April 1990*

The PDF of ϕ_x shown in Fig 4*b*, which is essentially a uniform distribution over $[-\pi, \pi]$, is typical for most natural terrain surfaces and volumes. If the cross-polarised scattering amplitude S_{hv} is statistically independent of S_{vv}, and since ϕ_{hv} and ϕ_{vv} are each uniformly distributed over $[-\pi, \pi]$, it can be easily shown that $\phi_x = \phi_{hv} - \phi_{vv}$ is uniformly distributed over $[-\pi, \pi]$.

However, the converse is not necessarily true; that is, if ϕ_x is uniformly distributed over $[-\pi, \pi]$, it does not necessarily follow that S_{hv} and S_{vv} are statistically independent.

Let us now return to further examination of the co-polarised phase difference ϕ_c. If S_{vv} and S_{hh} are totally uncorrelated, then

$$\lambda_{13} = \langle x_1 x_3 \rangle = 0 \tag{38}$$

$$\lambda_{14} = \langle x_1 x_4 \rangle = 0 \tag{39}$$

as a result of which we have $f(\phi_c) = 1/(2\pi)$, as expected. On the other hand, if the scattered wave always has the same polarisation independent of which segment area of the target is under observation, which implies that S_{vv} and S_{hh} are totally correlated, then the determinant of the covariance matrix given in Appendix 8 becomes zero and $f(\phi_c)$ becomes a delta function. For the general case, we can rewrite eqn. 36 in the form

$$f(\phi_c) = \frac{1-\alpha^2}{2\pi[1-\alpha^2\cos^2(\phi-\zeta)]} \times \left\{1 + \frac{a\cos(\phi-\zeta)}{\sqrt{[1-\alpha^2\cos^2(\phi-\zeta)]}} \times \left[\frac{\pi}{2} + \tan^{-1}\frac{\alpha\cos(\phi-\zeta)}{\sqrt{[1-\alpha^2\cos^2(\phi-\zeta)]}}\right]\right\} \tag{40}$$

where

$$\alpha = \sqrt{\left(\frac{\lambda_{13}^2 + \lambda_{14}^2}{\lambda_{11}\lambda_{33}}\right)} \tag{41}$$

$$\zeta = \tan^{-1}\frac{\lambda_{14}}{\lambda_{13}} \tag{42}$$

The parameter α, referred to as the degree of correlation [8], is a measure of the width of the PDF, and the parameter ζ is the value of ϕ_c at which $f(\phi_c)$ is a maximum. Fig. 6*a* shows plots of $f(\phi_c)$ for different values of ζ, with α held constant, and Fig. 6*b* shows plots of $f(\phi_c)$ for various values of α with ζ held constant. These two parameters completely specify $f(\phi_c)$.

3.3 The Mueller matrix

The Mueller matrix of a distributed target for which S_{hv} is uncorrelated with S_{vv} and S_{hh} contains only eight non-zero elements

$$\boldsymbol{M} = \begin{bmatrix} M_{11} & M_{12} & 0 & 0 \\ M_{21} & M_{22} & 0 & 0 \\ 0 & 0 & M_{33} & M_{34} \\ 0 & 0 & M_{43} & M_{M44} \end{bmatrix} \tag{43}$$

with four of them given by:

$$M_{11} = \langle |S_{vv}|^2 \rangle \tag{44}$$

$$M_{22} = \langle |S_{hh}| \rangle^2 \tag{45}$$

$$M_{12} = M_{21} = \langle |S_{hv}|^2 \rangle \tag{46}$$

Using eqns. 41 and 42 and the relations given in Appendix 8, the other four elements of $\boldsymbol{M}$, which are defined in eqn. 25, can be expressed in terms of the three principal magnitudes given by eqns. 44–46 and the parameters α and ζ

$$M_{33} = \alpha\cos\zeta\sqrt{(M_{11}M_{22})} + M_{12} \tag{47}$$

$$M_{44} = \alpha\cos\zeta\sqrt{(M_{11}M_{22})} - M_{12} \tag{48}$$

$$M_{34} = \alpha\sin\zeta\sqrt{(M_{11}M_{22})} \tag{49}$$

$$M_{43} = -\alpha\sin\zeta\sqrt{(M_{11}M_{22})} \tag{50}$$

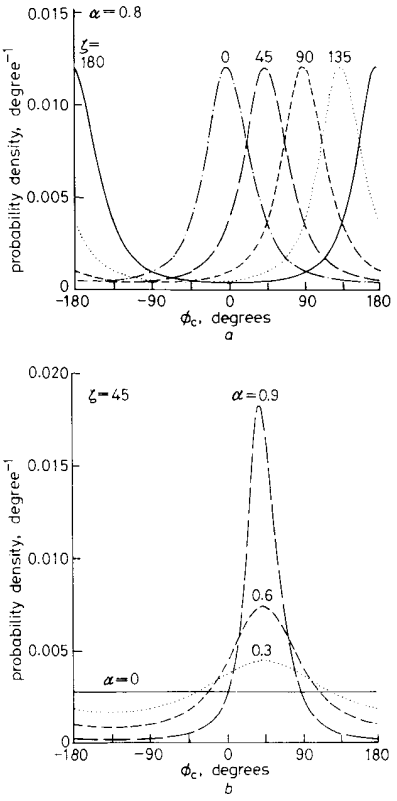

Fig. 6 *Plots of $f(\phi_c)$*
a various values of ζ at $\alpha = 0.8$
b various values of α at $\zeta = 45°$

3.4 Degree of polarisation

For a statistically homogeneous distributed target characterised by a Mueller matrix $\boldsymbol{M}$, illuminated by a modified Stokes vector $\boldsymbol{F}^i = [I_{vi}\, I_{hi}\, U_i\, V_i]^T$ and resulting in a backscattered modified Stokes vector $\boldsymbol{F}^s = [I_{vs}\, I_{hs}\, U_s\, V_s]^T$, in accordance with eqn. 24, the degree of polarisation of the backscattered wave is given by

$$m = \left[\frac{(I_{vs} - I_{hs})^2 + U_s^2 + V_s^2}{(I_{vs} + I_{hs})^2}\right]^{1/2} \tag{51}$$

As was noted earlier in Section 3.2, most natural targets exhibit the property that the crosspolarised scattering amplitude S_{hv} is uncorrelated with the co-polarised scattering amplitudes S_{vv} and S_{hh}, which leads to the result that eight of the elements of $\boldsymbol{M}$ are zero, as shown by eqn. 43. For this class of targets, m is given by

$$m = \left[\frac{a_1 I_{vi}^2 + a_2 I_{hi}^2 + a_3 U_i^2 + a_4 V_i^2 + a_5 I_{hi} I_{vi} + a_6 U_i V_i}{b_1 I_{vi}^2 + b_2 I_{hi}^2 + b_3 I_{vi} I_{hi}}\right]^{1/2} \tag{52}$$

where

$$a_1 = (M_{11} - M_{12})^2$$
$$a_2 = (M_{22} - M_{12})^2$$
$$a_3 = M_{33}^2 + M_{43}^2$$
$$a_4 = M_{34}^2 + M_{44}^2$$
$$a_5 = 2(M_{11} - M_{12})(M_{12} - M_{22})$$
$$a_6 = 2(M_{33} M_{34} + M_{43} M_{44})$$
$$b_1 = (M_{11} + M_{12})^2$$
$$b_2 = (M_{12} + M_{22})^2$$
$$b_3 = 2(M_{11} + M_{12})(M_{12} + M_{22})$$

Expressions for the non-zero elements of the Mueller matrix are given in Section 3.3 in terms of the magnitudes and phase parameters. Using the definition $\sigma_{ij}^\circ = (4\pi/A)\langle|S_{ij}|^2\rangle$ for the backscattering coefficient, we will now consider eqn. 52 for specific incident polarisations.

3.4.1 Vertical polarisation:

$\boldsymbol{F}_v^i = [1 \quad 0 \quad 0 \quad 0]^T$

$$m_v = \sqrt{\left(\frac{a_1}{b_1}\right)} = \frac{M_{11} - M_{12}}{M_{11} + M_{12}} = \frac{\sigma_{vv}^\circ - \sigma_{vh}^\circ}{\sigma_{vv}^\circ + \sigma_{vh}^\circ} \tag{53}$$

3.4.2 Horizontal polarisation:

$\boldsymbol{F}_h^i = [0 \quad 1 \quad 0 \quad 0]^T$

$$m_h = \sqrt{\left(\frac{a_2}{b_2}\right)} = \frac{M_{22} - M_{12}}{M_{22} + M_{12}} = \frac{\sigma_{hh}^\circ - \sigma_{vh}^\circ}{\sigma_{hh}^\circ + \sigma_{vh}^\circ} \tag{54}$$

3.4.3 Other polarisations: The following expressions apply to four different configurations of the polarisation state of the incident wave, in accordance with the following definitions of the coefficients *a–c*:

	a	*b*	*c*
45° linear	1	0	1
135° linear	−1	0	1
Right-hand circular	0	−1	−1
Left-hand circular	0	1	−1

$\boldsymbol{F}^i = [\frac{1}{2} \quad \frac{1}{2} \quad a \quad b]$

$$m = \left[\frac{(M_{11} - M_{22})^2 + 4[M_{12}^2 + M_{11}M_{22}\alpha^2 + 2cM_{12}\alpha\cos\zeta\sqrt{(M_{11}M_{22})}]}{(M_{11} + M_{22} + 2M_{12})^2}\right]^{1/2}$$
$$= \left[\frac{(\sigma_{vv}^\circ - \sigma_{hh}^\circ)^2 + 4[\sigma_{hv}^{\circ 2} + \sigma_{vv}^\circ\sigma_{hh}^\circ\alpha^2 + 2c\sigma_{hv}^\circ\alpha\cos\zeta\sqrt{(\sigma_{vv}^\circ\sigma_{hh}^\circ)}]}{(\sigma_{vv}^\circ + \sigma_{hh}^\circ + 2\sigma_{hv}^\circ)^2}\right]^{1/2} \tag{55}$$

According to the above expression, $m(45°) = m(135°)$ and $m(\text{RHC}) = m(\text{LHC})$.

4 Experimental observations of phase-difference statistics

The preceding section established that for random media for which the like- and crosspolarised scattering amplitudes are statistically uncorrelated, the Mueller matrix of the medium is completely specified by the three principal magnitudes, represented by the backscattering coefficients σ_{vv}°, σ_{hh}°, and σ_{vh}°, and two parameters, α and ζ, that characterise the probability density function of the co-polarised phase difference ϕ_c. The literature contains many examples, based on both theory and experimental observations, illustrating the relationships between the backscattering coefficients and the physical and dielectric properties of the target, but very few examples have been published on the behaviour of ϕ_c. In this section, we shall present examples of experimental measurements for a bare soil surface, a corn canopy, and small trees.

4.1 Bare-soil surface

Using a truck-mounted polarimetric scatterometer, backscatter measurements were conducted for four bare-soil fields with different surface roughnesses covering a 10 : 1 range in RMS height (0.32 cm to 3.2 cm). Each field was observed at 1.5, 4.75, and 9.5 GHz at multiple incidence angles extending from 20° to 70°, in 10° steps. A histogram of $f(\phi_c)$ for one of the fields was presented earlier in Fig. 4*a*. Whereas both the mean and standard deviation of ϕ_c, $\bar{\phi}_c$ and σ_{ϕ_c}, respectively, exhibit variations with surface roughness, incidence angle, and wavelength, the variations of $\bar{\phi}_c$ were relatively small in comparison with the variations observed for σ_{ϕ_c}. By way of example, we show in Fig. 7*a* plots of σ_{ϕ_c} as a function of incidence angle for a smooth surface at three frequencies, and plots for two different surface roughnesses at 1.5 GHz in Fig. 7*b*. The standard deviation σ_{ϕ_c}, or equivalently the parameter α defined by eqn. 42, is a measure of the degree of correlation between the co-polarised components of the scattering matrix. For the case of total correlation

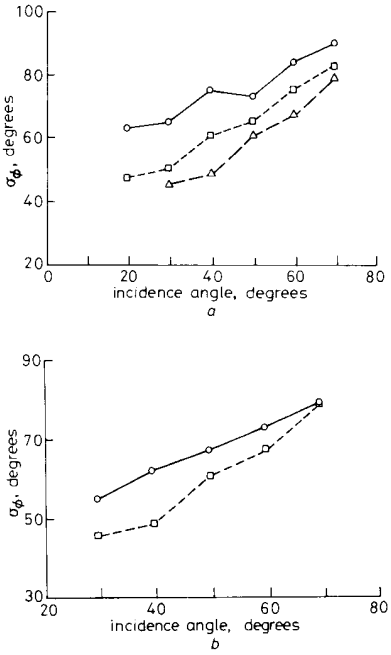

Fig. 7 *Standard deviation of the co-polarised phase angle as a function of incidence angle*

a a slightly rough field at three microwave frequencies
rms height = 0.32 cm
—○— 9.50 GHz
--□-- 4.75 GHz
—△— 1.50 GHz

b for two fields with very different surface roughnesses at 1.5 GHz
f = 1.5 GHz
—○— rms height = 0.32 cm
--□-- rms height = 3.02 cm

between S_{vv} and S_{hh}, $\sigma_{\phi_c} = 0$ and $\alpha = 1$, and for the opposite extreme of total uncorrelation, $\sigma_{\phi_c} = 104°$ and $\alpha = 0$. The results in Fig. 7 suggest that the degree of correlation decreases with increasing incidence angle and with increasing electromagnetic roughness $ks = 2\pi s/\lambda$, where s is the RMS height.

4.2 Corn canopy

Whereas $f(\phi_c)$ corresponding to a surface usually has a mean $\bar{\phi}_c$ that rarely exceeds 40°, $\bar{\phi}_c$ may be much larger for certain types of vegetation. A specific example is vegetation canopies comprised of plants with vertical stalks or trees with vertical trunks. Fig. 8 shows plots of $f(\phi_c)$

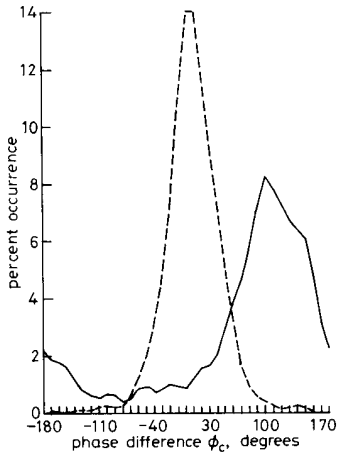

Fig. 8 *Measured co-polarised phase angle distributions for two corn fields observed by a 1.2 GHz polarimetric SAR at incidence angles of 19° and 50°*

for two fields of corn observed by a 1.2-GHz polarimetric SAR system that was flown over an agricultural area near McComb, Illinois. The swath width of the airborne SAR system covered an incidence-angle range extending from 15° to 55°. One of the fields represented in Fig. 8 was observed at an incidence angle of 19°, and the other at 50°. The mean values of ϕ_c are $\bar{\phi}_c = 9°$ for the first one and $\bar{\phi}_c = 109.5°$ for the second one. Similar distributions were extracted from the image for about 75 fields of corn. Fig. 9 shows the measured values of $\bar{\phi}_c$ for the corn fields, plotted against the incidence angle at which they were observed by the SAR. The solid curve, which provides a reasonable fit to the data, is based on direct calculations using the Michigan microwave canopy scattering model (MIMICS), which is a vector radiative transfer model for scattering from a vegetation canopy containing a trunk layer [3, 6]. The phase difference $\bar{\phi}_c$ includes the effects of propagation through a canopy containing vertical cylinders, reflection by the vertical cylinders, and reflection by the underlying ground surface. Each of these mechanisms introduces a polarisation-dependent phase shift. Through MIMICS, we can relate the mean co-polarised phase angle $\bar{\phi}_c$ to the biophysical parameters of the vegetation canopy. This is illustrated in Fig. 10 which shows a three-dimensional plot of $\bar{\phi}_c$ as a function of soil moisture content and stalk moisture content for a corn canopy observed at 1.2 GHz. We note that $\bar{\phi}_c$ appears to be essentially insensitive to soil moisture, but very sensitive to stalk moisture content. The *vv*-polarised backscattering coefficient, on the other hand, exhibits a strong

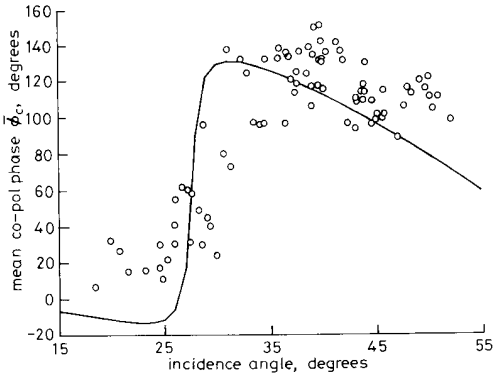

Fig. 9 *Measured and calculated mean co-polarised phase angle for corn fields observed by a 1.2 GHz SAR system*

○ Measured from SAR image
—— Calculated (MIMICS)

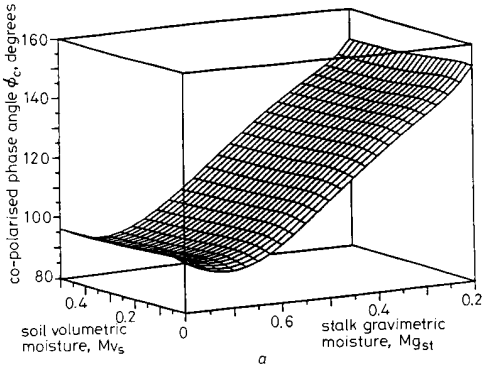

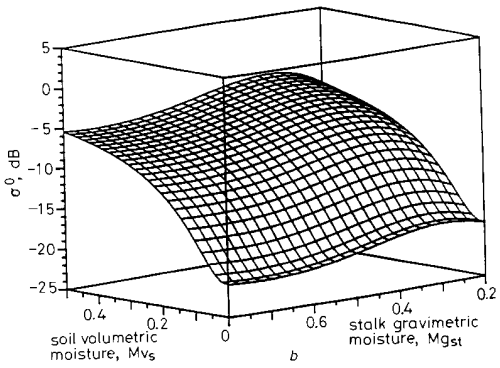

Fig. 10 *Variations*

a mean co-polarised phase angle
b vv-polarised backscattering coefficient with soil moisture content and stalk gravimetric moisture for a canopy of corn plants observed at 1.2 GHz at an incidence angle of 30°

dependence on soil moisture and only a weak dependence on trunk moisture. The combination of σ^0_{vv} and $\bar{\phi}_c$ can provide good estimates of both of these two physical properties of the corn canopy.

4.3 Small trees

A 35-GHz polarimetric scatterometer was used in an indoor facility to measure the backscatter from small trees. Fig. 11 compares the measured PDF of ϕ_c for a

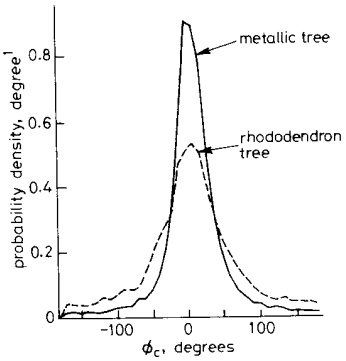

Fig. 11 *Measured $f(\phi_c)$ for a rhododendron tree and an artificial metallic tree at 35 GHz*

rhododendron tree, approximately 1 m in height, when observed along the broadside direction, with similar measurements for an artificial tree with metallic branches. This was part of a study to examine the variation of $f(\phi_c)$ with the dielectric properties of trees. The PDF of the metallic tree is much narrower than that of the rhododendron tree, with $\alpha = 0.89$ for the metallic tree, compared to $\alpha = 0.66$ for the real tree. Another example from the same study is presented in Fig. 12 in

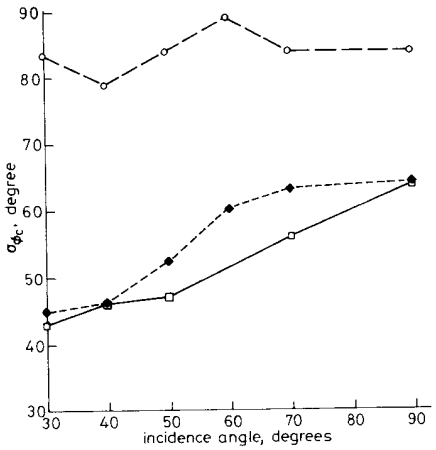

Fig. 12 *Measured standard deviation of co-polarised phase difference at 35 GHz for three types of tress*

—□— Rhododendron
--◆-- Spirea
—○— Spruce

which plots are shown for the standard deviation σ_{ϕ_c} as a function of incidence angle (with $\theta = 90°$ representing the broadside direction) for three types of small trees. We note that the spirea tree exhibits a distinctly different response from the rhododendron and spruce trees, which is attributed to the fact that the spirea tree is much denser than the other two.

At present, we are still in the early stage of developing an understanding of scattering by inhomogeneous media, particularly with regard to the statistics of the co-pol phase angle ϕ_c. The examples given in this section were merely intended to suggest that the mean value and standard deviation of ϕ_c, or alternatively the parameters α and ζ, may prove useful in providing information about the target over and beyond that provided by the backscattering coefficients alone. Hence, it is important to start examining the relationships between the statistical parameters of ϕ_c and the physical and dielectric properties of terrain through both theory and experimental observations.

5 Concluding remarks

The co-polarised phase angle ϕ_c is shown to be both sensor- and target-dependent. Its statistical properties vary with wavelength and incidence angle, surface roughness, type of vegetation cover, and vegetation geometry and biophysical properties. Further examination of the relationship between ϕ_c and the geometrical and dielectric properties of distributed targets, through both theoretical analyses and experimental observations, may lead to the development of novel tools for remotely sensing the Earth's surface with polarimetric radar systems.

6 Acknowledgment

This work was supported by NASA Grant NAGW-2151 and ARO Contract DAAL 03-91-G-0202.

7 References

1 ULABY, F.T., and ELACHI, C.: 'Radar polarimetry for geoscience applications' (Artech House, 1990)
2 VAN ZYL, J.J., ZEBKER, H.A., and ELACHI, C.: 'Imaging radar polarization signatures' theory and observation', *Radio Sci.*, 1987, **22**, pp. 529–543
3 ULABY, F.T., SARABANDI, K., McDONALD, K., WHITT, M., and DOBSON, C.: 'Michigan microwave canopy scattering model', *Int. J. Remote Sens.*, 1990, **11**, pp. 1223–1263
4 BORGEAUD, M., NGHIEM, S.V., SHIN, R.T., and KONG, J.A. 'Theoretical models for polarimetric microwave remote sensing of Earth terrain', *J. Electromagn. Waves and Appl.*, 1989, **3**, pp. 61–81
5 TSANG, L., and DING, K.H.: 'Polarimetric signatures of a layer of random nonspherical discrete scatters overlying a homogeneous half-space based on first- and second-order vector radiative transfer theory', *IEEE Trans.*, 1991, **GE-29**, pp. 242–253
6 McDONALD, K.C., DOBSON, M.C., and ULABY, F.T.: Using MIMICS to model L-band multiangle and multitemporal backscatter from a walnut orchard', *IEEE Trans.*, 1990, **GE-28**, pp. 477–491
7 ULABY, F.T., and DOBSON, M.C.: 'Handbook of radar scattering statistics for terrain' (Artech House, 1989)
8 SARABANDI, K.: 'Derivation of phase statistics of distributed targets from the averaged Mueller matrix'. Technical report 026511-T, 1991, Radiation laboratory, University of Michigan. Also accepted for publication in *Radio Science*
9 MEAD, J.B.: 'Polarimetric measurements of foliage and terrain at 225 GHz'. Ph.D. Thesis, Univ. of Mass., 1989
10 KUGA, Y., SARABANDI, K., NASHASHIBI, A., ULABY, F.T., and AUSTIN, R.T.: 'Millimeter wave polarimetric scatterometer systems: measurement and calibration techniques'. AGARD '91, 1991
11 ULABY, F.T., WHITT, M.W., and SARABANDI, K.: 'AVNA-based polarimetric scatterometers', *IEEE Antennas Propag. Mag.*, 1990, **32**, (5), pp. 6–17
12 SINCLAIR, G.: 'The transmission and reception of elliptically polarized waves', *Proc. IRE*, 1950, **38**, pp. 148–151
13 KENNAUGH, E.M.: 'Effects of the type of polarization on echo characteristcs'. Report 389–9, Antenna Laboratory, 1951, Ohio State University

8 Appendices

8.1 Probability density functions for co-pol and crosspol phase differences

8.1.1 Co-pol phase angle $\phi_c = \phi_{hh} - \phi_{vv}$: Let us define the complex scattering amplitudes S_{vv} and S_{hh} in terms of the real quantities $x_1, \ldots, x_4$

$$S_{vv} = |S_{vv}| e^{i\phi_{vv}} = x_1 + ix_2 \tag{56}$$

$$S_{hh} = |S_{hh}| e^{i\phi_{hh}} = x_3 + ix_4 \tag{57}$$

where

$$x_1 = |S_{vv}| \cos \phi_{vv} = \rho_1 \cos \phi_{vv} \tag{58}$$

$$x_2 = |S_{vv}| \sin \phi_{vv} = \rho_1 \sin \phi_{vv} \tag{59}$$

$$x_3 = |S_{hh}| \cos \phi_{hh} = \rho_2 \cos \phi_{hh} \tag{60}$$

$$x_4 = |S_{hh}| \sin \phi_{hh} = \rho_2 \sin \phi_{hh} \tag{61}$$

with $\rho_1 \triangleq |S_{vv}|$ and $\rho_2 \triangleq |S_{hh}|$. Since $x_1, \ldots, x_4$ are each zero-mean Gaussian random variables, their joint PDF is given by

$$f_{\boldsymbol{X}}(x_1, \ldots, x_4) = \frac{1}{4\pi^2 |\boldsymbol{\Lambda}|^{1/2}} \exp\left[-\tfrac{1}{2}\tilde{\boldsymbol{X}}\boldsymbol{\Lambda}^{-1}\boldsymbol{X}\right] \tag{62}$$

where $\boldsymbol{X}$ is the column vector

$$\boldsymbol{X} = \begin{bmatrix} x_1 \\ x_2 \\ x_3 \\ x_4 \end{bmatrix} \tag{63}$$

with transpose $\tilde{\boldsymbol{X}}$, and $\boldsymbol{\Lambda}$ is a 4×4 covariance matrix with elements

$$\lambda_{ij} = \lambda_{ji} = \langle x_i x_j \rangle, \quad i, j \in \{1, \ldots, 4\} \tag{64}$$

As was noted in Section 3.1, the real and imaginary parts of S_{vv}, x_1 and x_2, are mutually independent and identically distributed zero-mean random variables, and a similar statement applies to x_3 and x_4. Hence,

$$\lambda_{11} = \lambda_{22} = \langle x_1^2 \rangle = \langle x_2^2 \rangle = \tfrac{1}{2}\langle |S_{vv}|^2 \rangle = \frac{M_{11}}{2} \tag{65}$$

$$\lambda_{12} = \lambda_{21} = \langle x_1 x_2 \rangle = 0 \tag{66}$$

$$\lambda_{33} = \lambda_{44} = \langle x_3^2 \rangle = \langle x_4^2 \rangle = \tfrac{1}{2}\langle |S_{hh}|^2 \rangle = \frac{M_{22}}{2} \tag{67}$$

$$\lambda_{34} = \lambda_{43} = \langle x_3 x_4 \rangle = 0 \tag{68}$$

where M_{ij} is the ijth element of the Mueller matrix, as defined by eqn. 25. To characterise the remaining elements of the covariance matrix, we note that the absolute phase ϕ_{pp} is uniformly distributed over $[-\pi, \pi]$ and is independent of the magnitude $|S_{pp}|$. Hence, the random variable $(\phi_{vv} + \phi_{hh})$ is also uniformly distributed over $[-\pi, \pi]$ and is independent of $|S_{vv}||S_{hh}|$, from which we conclude that

$$\langle |S_{vv}||S_{hh}| \cos(\phi_{vv} + \phi_{hh}) \rangle = 0 \tag{69}$$

$$\langle |S_{vv}||S_{hh}| \sin(\phi_{vv} + \phi_{hh}) \rangle = 0 \tag{70}$$

From the definitions given by eqns. 58–61, and in view of eqns. 69 and 70, we obtain the results

$$\langle x_1 x_3 - x_2 x_4 \rangle = \langle |S_{vv}||S_{hh}| \cos(\phi_{vv} + \phi_{hh}) \rangle = 0 \tag{71}$$

$$\langle x_1 x_4 + x_2 x_3 \rangle = \langle |S_{vv}||S_{hh}| \sin(\phi_{vv} + \phi_{hh}) \rangle = 0 \tag{72}$$

which, in turn, lead to the relations

$$\lambda_{13} = \lambda_{24} \tag{73}$$

$$\lambda_{14} = -\lambda_{23} \tag{74}$$

From the definitions for the elements M_{33} and M_{44} of the Mueller matrix given by eqn. 25, their sum is given by

$$\begin{aligned} M_{33} + M_{44} &= 2\langle \mathrm{Re}\,(S_{vv} S_{hh}^*) \rangle \\ &= 2\langle |S_{vv}||S_{hh}| \cos(\phi_{vv} - \phi_{hh}) \rangle \\ &= 2\langle |S_{vv}||S_{hh}| \cos\phi_{vv} \cos\phi_{hh} \rangle \\ &\quad + 2\langle |S_{vv}||S_{hh}| \sin\phi_{vv} \sin\phi_{hh} \rangle \\ &= 2\lambda_{13} + 2\lambda_{24} \\ &= 4\lambda_{13} \end{aligned} \tag{75}$$

where use was made of eqn. 73. Hence,

$$\lambda_{13} = \lambda_{31} = \frac{M_{33} + M_{44}}{4} \tag{76}$$

We can similarly show that

$$\lambda_{14} = \lambda_{41} = -\lambda_{23} = -\lambda_{32} = \frac{M_{34} - M_{43}}{4} \tag{77}$$

Upon combining these relations between the elements of the covariance matrix and the elements of the Mueller matrix, we have

$$\boldsymbol{\Lambda} = \frac{1}{4}\begin{bmatrix} 2M_{11} & 0 & (M_{33} + M_{44}) & (M_{34} - M_{43}) \\ 0 & 2M_{11} & (M_{43} - M_{34}) & (M_{33} + M_{44}) \\ (M_{33} + M_{44}) & (M_{34} - M_{43}) & 2M_{22} & 0 \\ (M_{43} - M_{34}) & (M_{33} + M_{44}) & 0 & 2M_{22} \end{bmatrix} \tag{78}$$

With $\boldsymbol{\Lambda}$ known, let us now return to the joint density function of $\boldsymbol{X}$ given by eqn. (62) and use the rectangular to polar transformations given by eqns. 58–61 to obtain a joint density function for the magnitudes ρ_1 and ρ_2 and the phase angles ϕ_{vv} and ϕ_{hh}

$$\begin{aligned} &f_{\rho_1, \rho_2, \Phi_{vv}, \Phi_{hh}}(\rho_1, \rho_2, \phi_{vv}, \phi_{hh}) \\ &\quad = \frac{1}{4\pi^2\sqrt{(\Delta)}} \rho_1 \rho_2 \exp\{-\tfrac{1}{2}[a_1\rho_1^2 + a_2\rho_2^2 - 2a_3\rho_1\rho_2]\} \end{aligned} \tag{79}$$

where

$$\Delta = |\boldsymbol{\Lambda}| = (\lambda_{11}\lambda_{33} - \lambda_{13}^2 - \lambda_{14}^2)^2$$

$$a_1 = \lambda_{33}/\sqrt{\Delta}$$

$$a_2 = \lambda_{11}/\sqrt{\Delta}$$

$$a_3 = [\lambda_{13}\cos(\phi_{hh} - \phi_{vv}) + \lambda_{14}\sin(\phi_{hh} - \phi_{vv})]/\sqrt{\Delta}$$

To obtain the PDF of the co-polarised phase difference $\phi_c = \phi_{hh} - \phi_{vv}$, we first need to obtain the joint PDF of ϕ_{vv} and ϕ_{hh} from

$$\begin{aligned} &f_{\Phi_{vv}, \Phi_{hh}}(\phi_{vv}, \phi_{hh}) \\ &\quad = \int_0^\infty \int_0^\infty f_{\rho_1, \rho_2, \Phi_{vv}, \Phi_{hh}}(\rho_1, \rho_2, \phi_{vv}, \phi_{hh})\, d\rho_1\, d\rho_2 \end{aligned} \tag{80}$$

and after carrying out the integrations with respect to ρ_1 and ρ_2, we use a transformation to obtain $f(\phi_c)$. This

process, which is detailed in Reference 8, leads to

$$f(\phi_c) = \frac{\lambda_{11}\lambda_{33} - \lambda_{13}^2 - \lambda_{14}^2}{2\pi(\lambda_{11}\lambda_{33} - D^2)} \left\{1 + \frac{D}{\sqrt{(\lambda_{11}\lambda_{33} - D^2)}} \times \left[\frac{\pi}{2} + \tan^{-1}\frac{D}{\sqrt{(\lambda_{11}\lambda_{33} - D^2)}}\right]\right\} \quad (81)$$

where

$$D = \lambda_{13}\cos\phi_c + \lambda_{14}\sin\phi_c \quad (82)$$

The PDF given by eqn. 81 is completely specified by the elements of the covariance matrix Λ given by eqn. 72, all of which have been related to the elements of the Mueller matrix $\boldsymbol{M}$.

8.1.2 Cross-Pol phase angle $\phi_x = \phi_{hv} - \phi_{vv}$: The PDF for the cross-polarised phase angle ϕ_x can be obtained by following the same steps outlined in the preceding section for the co-polarised phase angle ϕ_c. If we define

$$S_{hv} = x_5 + ix_6 \quad (83)$$

and then repeat the steps of eqns. 58–81 with x_3 and x_4 replaced with x_5 and x_6, respectively, we obtain the PDF

$$f(\phi_x) = \frac{\lambda_{11}\lambda_{55} - \lambda_{15}^2 - \lambda_{16}^2}{2\pi(\lambda_{11}\lambda_{55} - D_1^2)} \left\{1 + \frac{D_1}{\sqrt{(\lambda_{11}\lambda_{55} - D_1^2)}} \times \left[\frac{\pi}{2} + \tan^{-1}\frac{D_1}{\sqrt{(\lambda_{11}\lambda_{55} - D_1^2)}}\right]\right\} \quad (84)$$

with

$$D_1 = \lambda_{15}\cos\phi_x + \lambda_{16}\sin\phi_x \quad (85)$$

and the elements λ_{11}, λ_{55}, λ_{15}, λ_{16} being related to the elements of the Mueller matrix by

$$\lambda_{11} = \frac{M_{11}}{2}, \quad \lambda_{55} = \frac{M_{12}}{2} \quad (86)$$

$$\lambda_{15} = \frac{M_{13}}{2}, \quad \lambda_{16} = \frac{M_{14}}{2} \quad (87)$$